

Development of a cryogenic microcalorimeter array for application in X-ray Astronomy

Marcel P. Bruijn,^{a*} Marcel L. Ridder,^a Eric Krouwer,^a Henk F.C. Hoevers,^a
Remco J. Wiegink,^b John J. van Baar,^b and Miko Elwenspoek^b

^a*SRON National Institute for Space Research, Sorbonnelaan 2, 3584 CA Utrecht, The Netherlands*

^b*MESA+ research institute, University of Twente, P.O. Box 217, 7500 AE Enschede, The Netherlands*

Received: 22 May 2003

Abstract

A report is presented on the development activities towards a cryogenic array of micro-calorimeters, based on voltage biased Ti/Au transition edge thermometers. The array, finally consisting of 32 x 32 sensors, is designed for application in the next generation X-Ray Astronomy missions, such as ESA's mission XEUS.

Recently SRON demonstrated a single pixel detector with an energy resolution $\Delta E_{\text{FWHM}} < 4$ eV at 5.9 keV combined with an effective time constant of 150 μs and a heat capacity which enables high x-ray absorption efficiency ($\geq 90\%$) at 5.9 keV. Presently arrays of 5 x 5 pixels are under development, as an intermediate step towards a final 32 x 32 pixel array.

Fabrication issues are discussed along the lines of two fabrication routes. One route utilizes bulk micromachining in [110] Si wafers, the other route surface micromachining with a sacrificial layer. The problems of dense electrical wiring and close packing of pixels are addressed, as well as thermal design issues.

Test structures and prototype 5 x 5 arrays have been fabricated and a preliminary cryogenic characterization was done.

The arrays have been designed with the aid of finite element simulation of the complete position dependent electrothermal behavior of a single pixel and thermal conductivity in the supporting structure. FEM simulation was also used for parameter extraction from measurements on the thermal test structures and estimation of electrical cross talk between pixels.

Keywords: Microcalorimeter; X-ray astronomy; imaging array; X-ray detector; cryogenic sensor; micro machining; XEUS.

1. Introduction

In the understanding of the evolution of the very early universe, X-ray astronomy plays a key role. It enables the study of hot baryonic matter, in particular the intra cluster medium, the true intergalactic medium, and massive black holes. Future space astronomy missions like XEUS are presently being defined and are based on high resolution X-ray spectroscopy with significantly improved sensitivity and imaging capabilities, compared to the present X-

ray observatories. Key elements are a huge X-ray mirror assembly and detectors with challenging specifications. The narrow field detectors (1 arcmin. field of view) for the energy range 0.1 to 30 keV should combine high resolution ($\Delta E_{\text{FWHM}} < 5$ eV for 5.9 keV photons and 2 eV for 1 keV photons), a time constant smaller than 100 μs , and high efficiency ($> 90\%$ up to 7 keV) with imaging capabilities of typically 32 x 32 pixels [1]. The type of detector, which is considered as most promising for the higher part of the energy range (> 1 keV), is an array of voltage biased superconducting transition edge microcalorimeters [2], operated at sub-Kelvin

* Corresponding author. Tel.: +31-30-2535638; fax: +31-30-2540860; e-mail: M.P.Bruijn@sron.nl.

temperatures. In section 2 we will address briefly the status of development of single pixel microcalorimeters. Section 3 will indicate the critical development areas for array structures, followed by a description of the processing routes under investigation in section 4. The elements from a study of thermal transport properties, essential for the operation and design, are discussed in section 5. Section 6 will focus somewhat more on the problem of on-chip wiring. Fabrication results and a preliminary cryogenic characterization will be shown in section 7.

2. Single pixel microcalorimeters

The basic physics and theoretical performance of a voltage-biased detector with a superconductor-to-normal phase transition thermometer (TES) are well established [2,3] and will not be repeated here. A short description of the operation principle is as follows, see also figure 1:

A microcalorimeter consists of a radiation absorber, which is weakly coupled to a cold bath and strongly coupled to a thermometer for readout of the temperature increase after absorption of a photon. Our thermometer is a bi-layer of a low temperature superconductor (Ti) and a normal metal (Au). The so-called proximity effect causes the transition temperature to be lower than that of the pure superconductor, and is typically 100 mK. The weak coupling to the bath temperature is obtained by placing the absorber and TES on a thin membrane of silicon-nitride, containing slots for tuning the conductance.

By using a constant voltage across the thermometer, instead of the conventional constant current, the device is used in the so called Extreme Electro Thermal Feedback (ETF) mode. After absorption the temperature rise causes a rise in resistance, which in its turn causes a decrease in current and therefore dissipated power in the sensor. This feedback mechanism increases the speed of response and partially cancels noise in the detector. In the extreme case almost all power is compensated by the current decrease, which makes the device self calibrating. Low noise read-out of the calorimeter is based on a Superconducting Quantum Interference Device (SQUID) pre-amplifier.

Some useful expressions are:

The energy resolution $\Delta E_{\text{FWHM}} = 2.36 \xi (k_B T^2 C)^{1/2}$, with k_B Boltzmann's constant, T the operating temperature and C the heat capacity of absorber and



Figure 1 Annotated micrograph of a single pixel X-ray microcalorimeter, used for explanation of the operation principle (see text).

thermometer. ξ is a factor depending on the steepness of the superconducting transition (resistance $R(T)$) of the TES, represented by $\alpha = d(\log R)/d(\log T)$, and the exponent n of the power law that governs the heat link (the power flow is proportional to $T^n - T_{\text{bath}}^n$). ξ is set point dependent and its typical value is about unity for representative microcalorimeters.

The effective time constant $\tau_e = (C/G)/(1+\alpha/n)$, where G is the thermal conductance to the bath. The effective time constant is shorter than the intrinsic time constant C/G due to electrothermal feedback in the sensor.

The best present sensors, as produced and measured at SRON have an energy resolution $\Delta E_{\text{FWHM}} = 3.9$ eV for 5.9 keV photons, combined with an effective time constant of 150 μs and 90% x-ray absorption efficiency [4]. This level of performance, very close to the theoretical limit, is amongst the best-reported values in literature [5, 6]. The experience with single pixel sensors, produced on large (4 mm square), closed silicon nitride membranes, forms the basis for the design of the array structures.

3. Microcalorimeter arrays

An imaging microcalorimeter could be constructed using two principles:

1. Intrinsic 1D or 2D sensors, based on thermal diffusion in a large absorber and using 2, respectively 4 thermometers per imaging element.
2. Pixel arrays.

Comparing the first scheme to the second, the energy resolution is degraded because of the larger heat capacity per imaging element and the achievable count rate will be considerably lower due to pile up of pulses. For the XEUS application a pixel array is a far better option, even when the increased readout complexity is taken into account.

The critical development areas of arrays have their origin in the following design constraints:

1. Each pixel should have the same thermal link to the heat bath.
2. Given the tight efficiency demands for XEUS, the filling factor must be $> 90\%$, so the pixel absorbers must be close packed.
3. The electrical and thermal cross talk between the pixels must be small enough not to degrade the energy resolution.
4. A process route must exist for a design.
5. The structure must survive handling, thermal cycling and vibrations during launch.

Constraint 1 sets serious limits to the lateral thermal gradients that are allowed in the pixel supporting structure. Because of insufficient knowledge and data in the literature of the relevant thermal transport properties of materials and interfaces at these low operating temperatures, some lithographic tunability must be built in. Characterization of thermal properties is an important development area; some more detail on this topic is presented in section 5.

Constraint 2 limits the available space for thermal connections and, more important, for electrical wiring. A schematic pixel design to tackle this problem is visible in figure 2. The absorber has been given a “mushroom” shape. These structures have been reported in [7] and SRON also showed promising single pixel response ($\Delta E_{FWHM}=5$ eV @ 5.9 keV) with such types of absorber [8]. A micrograph of this absorber is presented in figure 3.

The options which are presently under investigation to electrically connect a 32 x 32 pixel array are described in section 6.

Constraints 3 and 5 have not been studied experimentally so far. Instead we have made finite

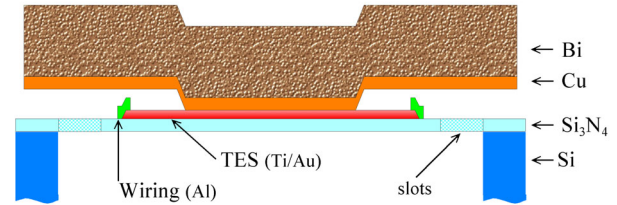


Figure 2 Schematic pixel design. A mushroom-shaped Cu/Bi absorber makes contact to the central part of a Ti/Au thermometer. A Si-nitride membrane contains slots for tuning the thermal conductivity as in figure 1. The Si support structure can be composed of long, narrow beams or part of a surface micromachined structure, see section 4.

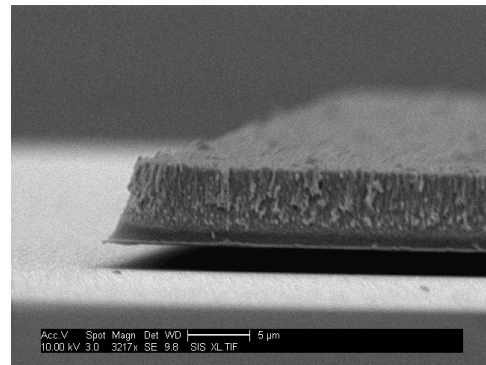


Figure 3 Outer part of a Cu/Bi absorber, hanging 1.3 μm above the surface.

element models (FEM) for both thermal and electrical cross talk. The estimated levels of cross talk will also be a drive for further development of the pulse processing algorithms. Moreover, the mechanical strength of etched nitride membranes was modeled using FEM, resulting in design guidelines. Experimental verification of these results is planned soon.

Two other important areas of development for the cryogenic sensor array are defined and under study:

- The read-out of the array is far from trivial. SQUID (Superconducting Quantum Interference Device) based pre-amplifiers must be specifically optimized for this application. For readout of large arrays, Time Domain Multiplexing [9] and Frequency Domain Multiplexing [10] are considered.
- For cooling of the sensor array a compact, rechargeable and space qualified ADR (Adiabatic Demagnetization Refrigerator) is under development.

4. Design and processing routes

For the 5 x 5 prototype sensor array two different processing routes will be pursued. The design of the thermometer, absorber and nitride cooling link is in principle identical for both routes, see figures 2 and 4. The thermometer, a Ti/Au bi-layer, has a critical temperature between 80 and 100 mK. The Bi absorber, with a thin Cu thermalization layer, is 7 μm thick.

The difference is the formation of the supporting structure. In route 1 this structure is formed by etching deep, vertical slots in the backside of a Si [110] wafer, using anisotropic wet etching, see figure 5. The resulting walls have a {111} orientation and a smooth surface.

In route 2 we create a shallow cavity underneath the membrane by surface micromachining techniques, using a poly-Si sacrificial layer, see figure 6. The cavity is opened at the end of the process, by wet TMAH etching from the front side or from the backside through a dry etched access hole. The advantage of route 2 is that it results in a structure with better thermal conductance and lower thermal cross talk. Furthermore the structure is mechanically more rigid and it opens the way for conducting the wiring under the pixel. The release process however has more uncertainties at the moment.

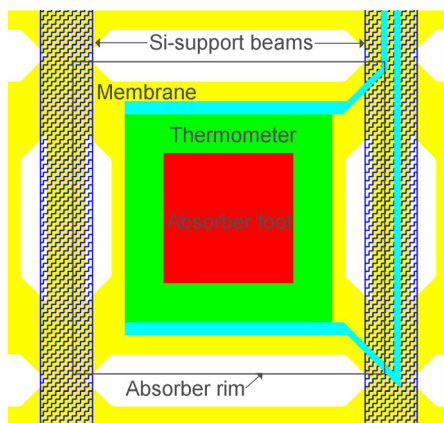


Figure 4 Basic layout of a sensor pixel (top view). The thermal conductance to the cold bath can be tuned by etching slots in a nitride membrane. The Si support beams under the membrane are either left after backside wet etching into a wafer, or thin deposited poly-Si ridges. For clarity only the two wiring lines to this pixel are drawn. Wiring from other pixels also runs along the beams.

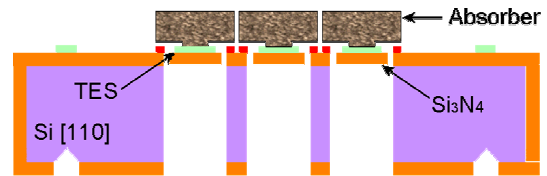


Figure 5 Schematic side view of a pixel array, formed by route 1. Slots are wet etched into a Si_3N_4 coated Si[110] wafer. The pixel structure on the top is formed by e-beam evaporation, sputter deposition, etching and lift-off processing techniques.

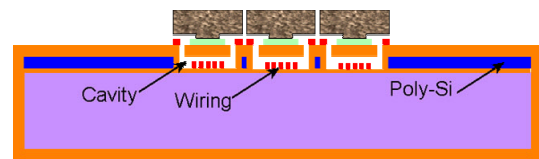


Figure 6 Schematic side view of a pixel array, formed by route 2. A poly-Si sacrificial layer is used to create a cavity under each pixel. Access to the cavity is either from top or bottom side (not shown in this figure).

5. Thermal transport at low temperatures

Following the route that the incoming X-ray power follows, we pass along the various development issues that are related to thermal transport.

1) The energy is absorbed by electrons in the absorber. The first transport mechanism is diffusion of heat within the electron system. In metals the thermal conductivity is strongly related to the electrical conductivity by Wiedeman-Franz's law. These parameters are easy to measure and no real development issue. Because the diffusion in pure Bi is relatively slow, a thin Cu layer is added for improvement. A typical diffusion time in the absorber becomes a few μs , fast compared to the desired timeconstant of the pixel (100 μs). This diffusion time sets the reaction time of the Ti/Au thermometer (together with the read out circuit).

2) Furtheron in the chain the heat will be conducted by insulators in the form of phonons. In the absorber/thermometer combination there must therefore be a transition of heat from the electron to the phonon system, the so-called electron-phonon coupling. From scattering theories [11, 12] a power law of heat transfer is predicted: $P = \Sigma V(T_e^n - T_{ph}^n)$ with a power coefficient n between 5 and 6. V is the volume and Σ a factor which is not known accurately for many materials.

3) At low temperatures heat cannot be exchanged freely between two different materials, because of quantisation of the frequency in the phonon spectrum. Depending on the difference in the velocity of sound, phonons have a chance of reflection at an interface. This effect is called the Kapitza resistance. The power transport (per interface area) also follows a power law with a coefficient $n \sim 4$ [13]. Experimental data is not widely available. We need to measure the effect for the materials and interfaces used at various places in the calorimeter structure.

4) From the metal part of the pixel to the supporting structure the heat is transported by diffusion in a structured silicon nitride membrane. The thermal conductivity is thickness dependent and for narrow lateral geometries also geometry dependent. Experimental data is available [14, 15] but need to be refined for our particular situation. We plan to measure the thermal conductivity on structures resembling the pixel layout, using tiny heaters and (superconducting tunnel junction based) thermometers, fabricated on the surface.

5) Referring to constraint 1 in section 3, a good thermal transport in the support structure is very important. At sub-Kelvin temperatures, in dielectric solids, the heat conduction by phonons can become dominated by scattering from surfaces, when the mean free path for scattering at bulk impurities and defects becomes comparable or larger than sample dimensions. Depending on the roughness of the surfaces, phonons scatter diffusively or specularly. The latter mode, also called ballistic transport, is preferred.

The thermal conductivity of Si-beams, fabricated using route 1, was measured, using a setup as presented in figure 7. The results were analyzed by comparing the experimental temperatures to a modeled profile. We have proposed a description, using the mean free path, to treat surface scattering by finite element modeling of heat flow in micromachined structures [16]. The phonon mean free path obtained from these data ($150 \pm 50 \mu\text{m}$), indicates a cross-over from diffuse to specular phonon reflection. These preliminary results enable us to model the thermal performance of our array sensors. More accurate thermal measurements, where the Ti/Au bi-layer thermal switches are replaced by tunnel junction based continuous thermometers are planned for the near future.

6) Finally the heat needs to be transferred from the detector chip to the Cu-cooling bracket of the cryostat. Several of the above mentioned

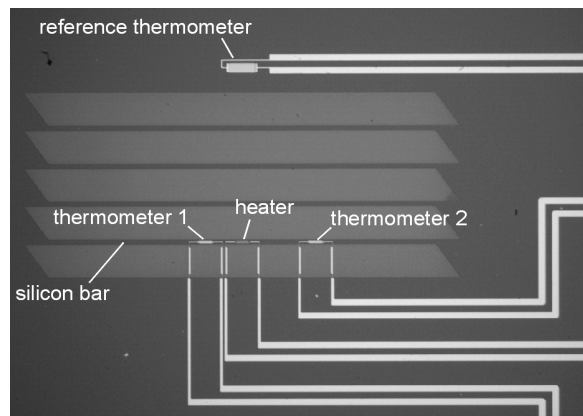


Figure 7 Photograph of an experimental device. On one of the $40 \mu\text{m}$ wide etched Si-bars, a Cu heater and two Ti/Au bi-layer thermometers were lithographed. After cool down to a base temperature of 20 mK, the power through the heater is varied and the thermometers are heated to the normal state.

mechanisms play a role. A proper mounting method needs to be developed and tested.

A finite element model of a pixel has been constructed, which includes the effects mentioned under 1) to 4) above [17]. The full electrothermal response, dependent on the impact position of the X-ray photon, can be simulated. It also includes the electronic biasing circuit. Together with separate 2- or 3-dimensional models of the transport in the support structures, it forms an important tool in the design of a complete array. The accuracy of the design is of course related to the accuracy with which the various material- and interface parameters described in this section are known.

6. On-chip electrical wiring

Depending on the readout circuit each pixel needs to be connected with one or two wires to the perimeter of the chip, the former case when a common return is used. Even in this case the wiring density will be high when only the narrow beams of the supporting structure can be used. For these double sided processes 1:1 contact lithography is the only choice, so the lithographic resolution will be somewhere around $1 \mu\text{m}$.

We have done an inventory study of the possible options for on-chip wiring and have presently chosen the following options to investigate further:

1) Multilayer wiring, separated by insulating layers.

2) Separation of the detector into two chips with partly covering of the surface area, see figure 8. This

is an option for the XEUS detector because the optical system has a large focal depth of several mm.

3) The surface micromachining fabrication route opens another option: we can use the area under the pixel. The wiring can be fabricated before the sacrificial layer is deposited and be contacted by etching vias after fabrication of the thermometers. A schematic view of this option is given in figure 6 (side view) and figure 10 (top view).

Common development issues for all wiring technology are good processes for insulation and crossing steps. The latter often causes a reduced critical current carrying capability for narrow superconducting lines. Planarization processes using chemical mechanical polishing might be required.

Referring back to constraint 3 in section 3, questions arise about the electrical cross talk due to these narrow spaced lines. A finite element simulation study was done and basic values for capacitance, self inductance and mutual inductance were calculated for the different options. These values can be inserted in other circuit simulation software to estimate the crosstalk in the total readout circuit. An important conclusion was that for all wiring magnetic screening is necessary, by using a separate microstripline design or a common groundplane close under the lines. For clarity this has not been implemented in the schematic figures in this article.

7. Array fabrication results

Recently the first operating prototype arrays have been fabricated by the SRON-MESA collaboration. A micrograph is presented in figure 10. This array was processed using the bulk micromachining route. Because of limitations in our present characterization setup, not all pixels have been wired to the perimeter. Instead we have chosen to read out three representative pixels, one in the center, one at the edge and one in the corner of the array. The other pixels are connected in parallel so that bias power can be applied across the whole array. This array contains Cu absorbers with the same heat capacity as required for full covering, 7 μm thick Bi absorbers.

We measured the transition temperature, current-voltage characteristics and power plateau (power which drives the thermometer in the upper region of the transition) as a function of bath temperature. The results were very similar for the three pixels. The power plateau is unexpected high. We can model the results with a thermal conductivity 6 times as high

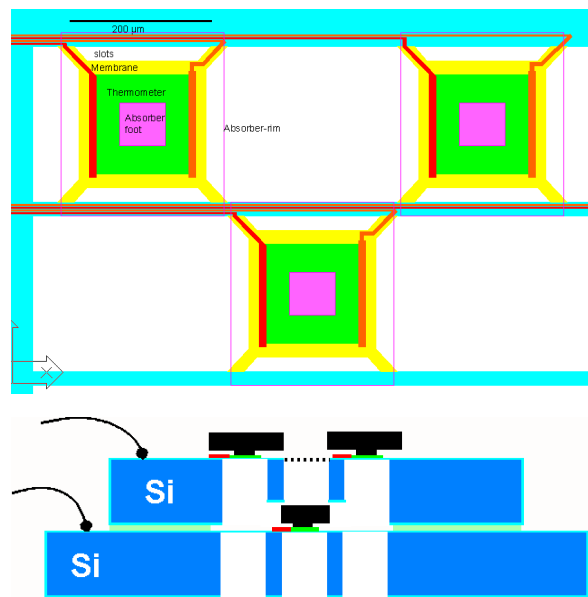


Figure 8 Schematic top view and side view of a proposed option to reduce the wiring density for a close-packed pixel array. A detector is split into two chips, the pixels are arranged in a checkerboard layout.

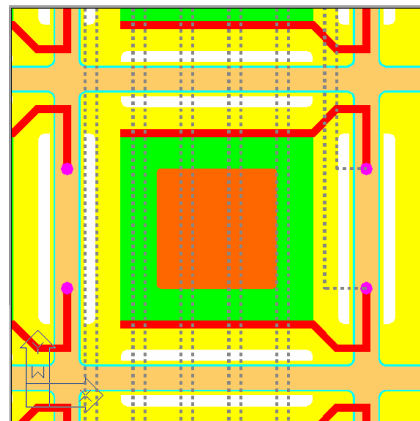


Figure 9 Schematic representation of wiring option 3) with wires (dashed lines) running under the pixel. The lines are connected to the pixel wiring (red lines) at the side of the pixel by etched vias.

as used for fitting earlier single pixel calorimeters. A systematic study is planned using arrays with different etched patterns in the nitride layer and special test structures to test the issues described in section 5. Furthermore a preliminary characterization of the X-ray response (5.9 keV photons) was done. For one of the arrays an energy resolution of 10 eV was measured. This value is twice as high as for the best single pixel detector. The resolution is degraded

by an excess of low frequency noise, presumably an experimental effect, which is under study.

With the surface micromachining route we did not fabricate working prototypes yet. The support structure however has been fabricated separately, see figure 11. It has been tested separately that the process of etching the cavity when the rest of the metal layers are present can be done without affecting the superconducting properties of the thermometer. A full prototype will be fabricated soon.

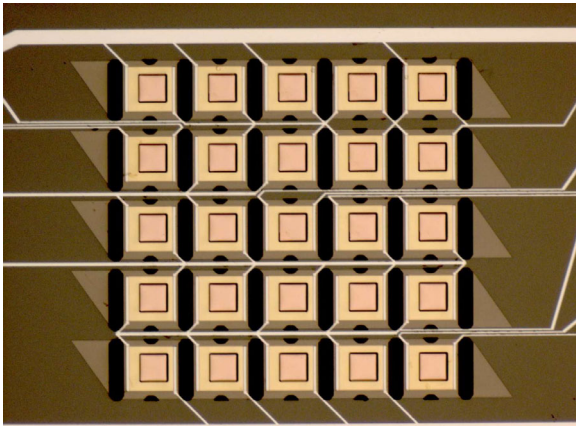


Figure 10 Prototype calorimeter array, fabricated using the bulk micromachining route.

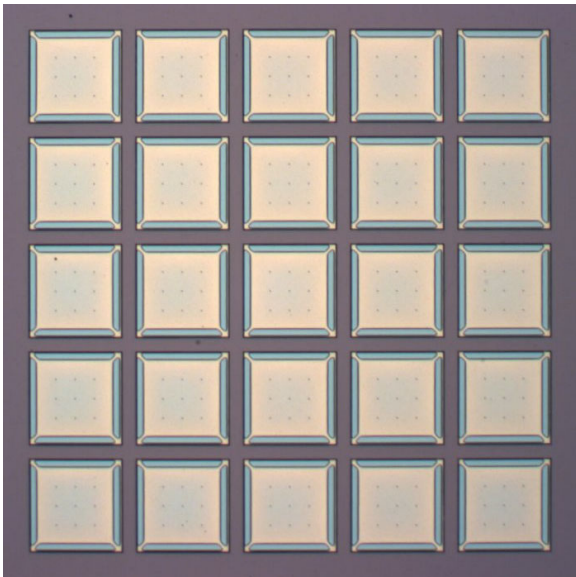


Figure 11 Support structure for a calorimeter array, fabricated using the surface micromachining route. Membranes are free hanging above a cavity formed by etching a poly-Si sacrificial layer. The nine tiny bumps in each pixel are used to prevent sticking of the membrane to the bottom of the cavity

Key to this process is the use of tiny bumps to prevent sticking of the membrane to the bottom of the cavity. This is illustrated in figure 12. The sidewalls of the cavity are formed by etching narrow slots in the poly-Si sacrificial layer, which are filled during deposition of the top layer of Si-nitride, which will form the membrane. A detail of this part of the process is presented in figure 13.

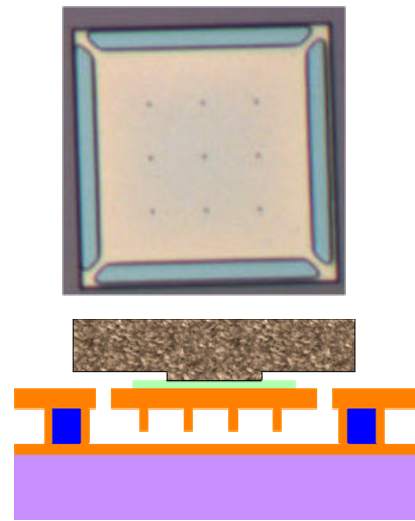


Figure 12 Enlarged pixel from figure 11 and a schematic side view of the cavity with nitride bumps and sidewalls to prevent etching of ridges of poly-Si (blue) at the side of the pixels. The metal layers in the schematic view have not yet been integrated.

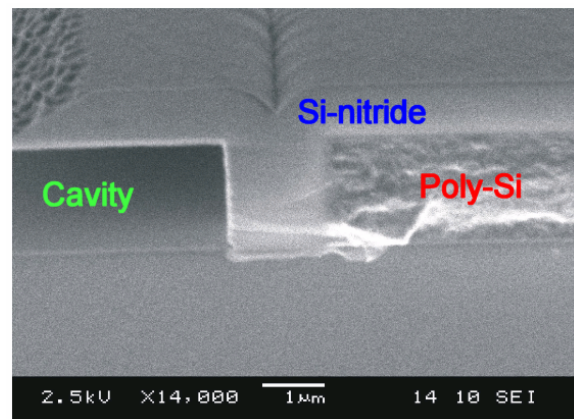


Figure 13 Detail of the sidewall of the cavity under a pixel. The Si-nitride fills a narrow slot in the poly-Si sacrificial layer

8. Concluding remarks

- In this paper, we have presented our development activities of microcalorimeter arrays, which have high potential for future high resolution imaging X-ray spectroscopy.
- Prototype 5x5 arrays enter the characterization phase.
- For a proper design however, several thermal transport issues need to be solved.
- (Finite element) modeling tools are ready for optimization.
- A high on-chip electrical wiring density sets processing challenges.
- Two promising processing routes still feasible.

Acknowledgments

Part of this work is supported by a research grant from the Nederlandse Organisatie voor Wetenschappelijk Onderzoek (NWO), and by a contract of the ESA technological research programme for the development of an imaging microcalorimeter array for XEUS.

References

- [1] P.A.J. de Korte et al., SPIE Proc. 3766 (1999) 103.
- [2] K.D. Irwin, Appl. Phys. Lett. 66 (1995) 1998.
- [3] K.D. Irwin, G.C. Hilton, D.A. Wollman, and J.M. Martinis, J. Appl. Phys. 83 (1998) 3978 .
- [4] W.M. Bergmann Tiest, H.F.C. Hoevers, M.P. Bruijn, W.A.Mels, M.L. Ridder, P.A.J. de Korte, and M.E. Huber, Proc. 9th Int. Workshop on Low Temperature Detectors, Madison, 22-27 July 2001, AIP Conf. Proc. 605 (2002) 199.
- [5] K.D. Irwin, G.C. Hilton, J.M. Martinis, S. Deiker, N. Bergren, S.W. Nam, D.A. Rudman, and D.A. Wollman, Nucl. Instr. Meth. A 444 (2000) 184.
- [6] C.K. Stahle, P. Brekosky, E. Figueroa-Feliciano, F.M. Finkbeiner, J.D. Gygax, M.J. Li, M.A. Lindeman, F. Scott Porter, and N. Tralshawala, SPIE Proc. 4140 (2000) 367.
- [7] N. Tralshawala et al. Nucl. Instr. Meth. A 444 (2000) 188.
- [8] W.M. Bergmann Tiest et al., NIST workshop on noise in TES microcalorimeters, April 25, 2002, unpublished.
- [9] K.D. Irwin, Physica C 368 (2002) 203.
- [10] M. Kiviranta, H. Seppä, J. van der Kuur, and P. de Korte, Proc. Far IR, sub-mm and mm Detector Technology Workshop, Monterey 1 – 3 April 2002, to be published.
- [11] F.C. Wellstood, C. Urbina and J. Clarke, Phys. Rev. B 49 (1994) 5942.
- [12] A. Sergeev and V. Mitin, Phys. Rev. B 61 (2000) 6041.
- [13] F. Pobell, *Matter and Methods at Low Temperatures*, (Berlin: Springer) (1992).
- [14] W. Holmes, J.M. Gildemeister, P.L. Richards, V. Kotsubo, Appl. Phys. Lett. 72 (1998) 2250.
- [15] M.M. Leivo and J.P. Pekola, Appl. Phys. Lett. 72 (1998) 1305.
- [16] Z. Moktadir, M.P. Bruijn, R. Wiegerink, M. Elwenspoek, M. Ridder, W.A. Mels, Proc. IEEE Sensors 2002, paper 37.3, Orlando, 11 –14 June, 2002.
- [17] Software and support: FEMLAB 2.3, Comsol AB.